IEEE Access
Multidisciplinary | Rapid Review | Open Access Journal

Received December 18, 2018, accepted January 12, 2019, date of publication January 22, 2019, date of current version February 8, 2019.

Digital Object Identifier 10.1109/ACCESS.2019.2894167

Analytical Approach of Director Tilting in Nematic Liquid Crystals for Electronically Tunable Devices

ANTONIO ALEX-AMOR[1,2] ADRIÁN TAMAYO-DOMÍNGUEZ[2], ÁNGEL PALOMARES-CABALLERO[1,3], JOSÉ M. FERNÁNDEZ-GONZÁLEZ[2], PABLO PADILLA[3], JUAN VALENZUELA-VALDÉS[3], AND ANTONIO PALOMARES[4]

[1]Departamento de Lenguajes y Ciencias de la Computación, Universidad de Málaga, 29071 Málaga, Spain
[2]Information Processing and Telecommunications Center, Universidad Politécnica de Madrid, 28040 Madrid, Spain
[3]Departamento de Teoría de la Señal, Telemática y Comunicaciones, Universidad de Granada, 18071 Granada, Spain
[4]Departamento de Matemática Aplicada, Universidad de Granada, 18071 Granada, Spain

Corresponding author: Antonio Alex-Amor (aalex@gr.ssr.upm.es)

This work was supported in part by the Spanish Research and Development National Program under Project TIN2016-75097-P, and in part by the Ministerio de Economía under Project TEC2017-85529-C3-1-R.

ABSTRACT This paper presents an analytical expression that models the tilt angle of directors in a nematic liquid crystal (LC), depending on its elastic properties, its dielectric anisotropy, and the quasi-static electric field applied. The analytical solution obtained is fast and easily computable in comparison with numerical estimations and is of special interest in radiofrequency; for instance, for the LC modeling in full-wave electromagnetic simulators in the design process of electronically tunable devices, such as microwave phase shifters or electronically steerable antennas for satellite communications. Subsequently, a comparison is made between numerical approaches (self-implemented shooting method) and the analytical formulas when varying the parameters of the LC, being demonstrated its usefulness. The average LC director is then obtained and used to form the full permittivity tensor that completely characterizes the electrical properties of the material. Finally, an electromagnetic simulation is carried out to show the capabilities of the LC as a tunable phase shifter. It is shown that only 5 cm of a commercial 200-μm LC mixture is necessary to achieve 360° of the maximum variable phase shift at the 30-GHz band.

INDEX TERMS Liquid crystal, nematic phase, analytical expression, microwave, phase shifting.

I. INTRODUCTION

Of the most impacting technologies created over the past thirty years, mobile communications is one of the most prominent. The demand for a higher quality of service, throughput, and efficiency has led to exploring new frequency ranges, new technologies, and new materials. It has led to the fifth generation of mobile communications (5G). Controlling the radiation parameters of the antennas is one of the critical technological challenges that have arisen, since adaptive beamforming is expected to play an important role in 5G networks [1]. For this reason, new materials such as graphene [2], ferroelectrics [3] or liquid crystal (LC) [4] are beginning to be used for the design of microwave tunable devices.

The design of devices based on liquid crystal substrates with electronically controllable permittivity allows their phase response to be controlled. That property converts the LC into a substitute for other components, such as varactors, PIN diodes or ferrites. Electronic phase control is a key factor in radiofrequency, as it permits controlling the propagation direction and reconfiguration of the main beam in communication systems [5], [6]. For instance, Perez-Palomino *et al.* [7] use the dielectric anisotropy of the liquid crystal to design a reconfigurable reflectarray. The results show that the prototype operates from 96 to 104 GHz with an astonishing performance. On the other hand, Karabey *et al.* [8] present a 2-D electronically steered phased array antenna based on microstrip patches. The array is fed through a tunable spiral-shape line suspended on liquid crystal, which offers a phase shift up to 300° when polarizing the LC from 0 to 15 Volts. Hu *et al.* [9] create a frequency selective surface (FSS) that implements a 140 GHz tunable bandpass filter based on the use of a 10 Volts polarized liquid crystal. They also demonstrate the potential to transform the FSS into a reflecting structure (a notch filter). As a last example, new trends are trying to exploit the concepts of

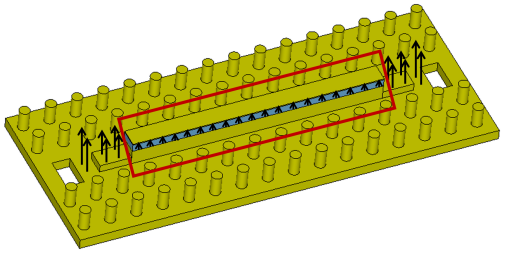

FIGURE 1. Ridge gap waveguide to exploit the phase shift provided by a liquid crystal confined between two metallic plates (marked in red). The electric field appears marked in black.

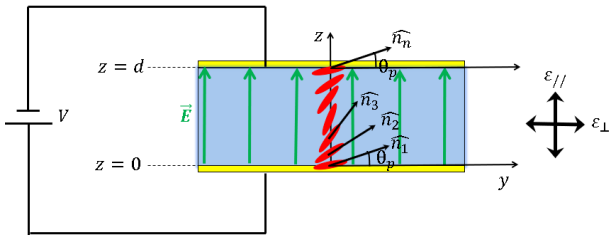

FIGURE 2. Director distribution in a nematic liquid crystal enclosed by two metallic plates.

groove/ridge gap waveguide [10], [11] to design novel phase shifters that make use of liquid crystal, typically confined between two parallel plates. Figure 1 depicts more clearly a possible design, based on the use of ridge gap waveguide. The ridge progressively confines the electric field into the liquid crystal and the anisotropy of the LC is used to control the phase shift in the structure.

The equations that rule the behavior of the liquid crystal typically lacks an analytical solution. Thus, finite difference (FDM) and finite element (FEM) methods are commonly used to obtain numerical approaches. For instance, finite difference and Runge-Kutta algorithms are applied in [12] in order to model the relaxational dynamics of liquid crystals under applied electric fields. Likewise, the finite difference method is used in [13] to solve the equations of the Ericksen-Leslie dynamic theory. On the other hand, 2D and 3D finite element methods are used in [14] and [15], respectively, to model the non-uniform electric and director fields in the liquid crystal. More recent studies have made use of a finite-difference frequency-domain method [16] and a finite element method [17] to analyze diffraction effects and wave propagation through liquid crystal devices. Another numerical approach to solve boundary problems like this one makes use of the shooting method (depicted in section IV.C). Thus, Guan *et al.* [18] obtain the response times in liquid crystal displays. A numerical comparison among the use of the shooting method, the FDM, and the Matlab bvp4c solver is presented in [19].

In this paper, we propose an analytical expression that models the behavior of a LC confined between metallic plates. This analytical expression substantially accelerates any electromagnetic simulation that makes use of this novel tunable material. The document is therefore organized as follows: Sections I and II introduce the main characteristics of the liquid crystal and its use as a tunable device. Section III focuses on simplifying the differential equation that models the tilt angle of directors in the LC. Section IV presents the analytical solution and a comparison with a self-implemented shooting method. Section V describes throughout an example how to properly use the analytical expression in practice. Section VI is reserved to study the use of the liquid crystal as a phase shifter in a full wave electromagnetic simulator. Finally, conclusions are drawn in Section VII.

II. BASIC PROPERTIES OF A NEMATIC LIQUID CRYSTAL CONFINED BETWEEN METALLIC PLATES

There exist several phases in which liquid crystal can be found. One of the most common used in microwave is the nematic phase, wherein the molecules are oriented in the same average direction. Therefore, as shown in Fig. 2, from the definition of the directors $\hat{n}_i$, most properties of liquid crystal can be studied, as for example its dielectric anisotropy. For its proper characterization, it is especially important to know how directors are oriented in the liquid crystal along the direction z, that is, $\theta(z)$. Once determined, its average director tilt angle θ_m is used to form the full permittivity tensor $\bar{\bar{\varepsilon}}$ that completely characterizes the material, and allows to study its properties as a phase-shifting element in a full-wave electromagnetic simulator.

When the LC is confined between two parallel metallic plates and an uniform z-oriented quasi-static electric field is applied on it ($\vec{E} = E_o\hat{z}$), the molecules are free to rotate in the Y-Z plane and the permittivity tensor can be expressed as

$$\bar{\bar{\varepsilon}} = \begin{pmatrix} \varepsilon_\perp & 0 & 0 \\ 0 & \varepsilon_\perp + \Delta\varepsilon\cos^2(\theta_m) & \Delta\varepsilon\sin(\theta_m)\cos(\theta_m) \\ 0 & \Delta\varepsilon\sin(\theta_m)\cos(\theta_m) & \varepsilon_\perp + \Delta\varepsilon\sin^2(\theta_m) \end{pmatrix} \quad (1)$$

where $\varepsilon_\perp$ is the perpendicular permittivity, $\varepsilon_{//}$ is the parallel permittivity, and $\Delta\varepsilon = \varepsilon_{//} - \varepsilon_\perp$ is the dielectric anisotropy [20]–[22]. These parameters are specific to each material. When an elevated quasi-static electric field is applied (a high potential drop), the molecules tend to be oriented perpendicularly to the metallic plates, whereas when this electric field is reduced or null, the molecules are oriented parallel to the metallic plates. Additionally, the plates physically impose the molecules to be placed parallel to them at their interfaces with the liquid crystal, $z = 0$ and $z = d$.

The average behavior of molecules in a liquid crystal confined between metallic plates is modeled according to differential equation (2), which is presented in section III. Because there is no analytical expression that satisfies our requirements, we are forced to perform numerical analysis in order to obtain the solution sought. This is tedious in this particular case and may be of relative difficulty.

III. THE DIFFERENTIAL EQUATION

The differential equation that models the director variation in a liquid crystal (LC) in the nematic phase as a conse-

quence of the application of a uniform quasi-static electric field (electric-field-induced splay Fréedericksz transition [23]) was presented in [24] as

$$\left(k_{11}\cos^2\theta + k_{33}\sin^2\theta\right)\frac{d^2\theta}{dz^2} + (k_{33}-k_{11})\left(\frac{d\theta}{dz}\right)^2\sin\theta\cos\theta + \beta\sin\theta\cos\theta = 0 \quad (2)$$

where k_{11} and k_{33} are elastic constants, $\beta = \varepsilon_0\Delta\varepsilon E^2$, $\varepsilon_0 = 8.85\cdot10^{-12}$ F/m is the vacuum permittivity, $\Delta\varepsilon = \varepsilon_{//} - \varepsilon_{\perp}$ is the liquid crystal dielectric anisotropy, E is the module of the quasi-static electric field applied and $\theta(z)$ is the director tilt angle, in regard to direction z. Note that the fringing effect [25] is not included in the definition of equation (2), since an uniform z-oriented electric field (Fig. 2) has been considered.

Equation (2) is subject to the boundary conditions $\theta(z = 0) = \theta_p = \theta(z = d)$, where θ_p is named as pretilt angle. It is a second order strongly nonlinear differential equation that lacks an analytical solution. The simplest simplification that can be done consists in linearizing equation (2) considering only small angles. Therefore, (2) turns into a second-order linear differential equation, whose solution is a well-known expression. It is clearly depicted in [24] and [26]. Regretfully, this analytical solution only offers good results when considering small tilt angles, which will not be our particular case.

If we divide both terms of (2) by $\cos^2\theta$ and apply the change of variable $t = \tan\theta$, with $\frac{d\theta}{dz} = \left(\frac{1}{t^2+1}\right)\frac{dt}{dz}$, we can rewrite (2) in terms of t as

$$\left(k_{11}+k_{33}t^2\right)\left(\frac{1}{t^2+1}\right)\frac{d^2t}{dz^2} + (k_{33}-k_{11})\left(\frac{t}{\left(t^2+1\right)^2}\right)\left(\frac{dt}{dz}\right)^2 + \beta t = 0 \quad (3)$$

With the quasi-static assumption ($E = V/d$), the electric field is directly related to the bias voltage V, and as V increases, the molecules tend to be oriented perpendicularly to the metal plates, that is, $\theta = 90°$. In most general cases, we are pretending to work with a high bias voltage, so $\theta(z) \to 90°$ and $t = \tan\theta$ becomes big enough. In consequence $\frac{t}{(t^2+1)^2} << \frac{1}{t^2+1} << t$, and therefore the term $(k_{33}-k_{11})\left(\frac{t}{(t^2+1)^2}\right)\left(\frac{dt}{dz}\right)^2$ can be neglected from equation (3). Operating and separating into simple fractions, the differential equation (3) can be rewritten as

$$\frac{d^2t}{dz^2} = -A\left(t + \frac{t\,(1-a)}{t^2+a}\right) \quad (4)$$

where $A = \frac{\beta}{k_{33}}$ and $a = \frac{k_{11}}{k_{33}}$. A particular case appears when $a = 1$ ($k_{11} = k_{33}$). That is the situation for a variety of commercial LC substrates. In this case, the term $\frac{t(1-a)}{t^2+a}$ vanishes directly. Thus, equation (4) is simplified in the domain of $\theta(z)$ to

$$\frac{d^2\theta}{dz^2} = -\frac{A}{2}\sin(2\theta) \quad (5)$$

Under normal circumstances, both elastic constants are very similar in their values. For example, in the 75-μm thick LC-layer LC GT3-23001 [20] the elastic constants are $k_{11} = 24$ pN and $k_{33} = 34.5$ pN, which means $a = 0.696$. On the other hand, in the LC mixture MCL-6608, used in [26], the elastic constants $k_{11} = 16.7$ pN and $k_{33} = 18.1$ pN are even more similar to each other, giving a value of $a = 0.923$.

IV. ANALYTICAL SOLUTION

Once simplified the original differential equation, it would be desirable to find an analytical solution of its approximation (5). So, we define a new change of variable $w = \frac{d\theta}{dz}$, with $\frac{d^2\theta}{dz^2} = w\frac{dw}{d\theta}$. In these terms, equation (5) can be rewritten as

$$w\frac{dw}{d\theta} = -\frac{A}{2}\sin(2\theta) \quad (6)$$

where the variables w and θ can be separated from each other. Integrating both sides of the equation leads to

$$w = \pm\sqrt{A\cos^2\theta + c_1} \quad (7)$$

Within $w = \frac{d\theta}{dz} = \pm\sqrt{A\cos^2\theta + c_1}$, we can separate again the variables z and θ. If we integrate both members of the equation and then operate, we obtain that

$$z + c_2 = \pm\frac{1}{\sqrt{A+c_1}}\int\frac{1}{\sqrt{1-\frac{A}{A+c_1}\sin^2\theta}}\,d\theta \quad (8)$$

From [27], we know that $\mathrm{F}\left(\theta\,|\,k^2\right) = \int_0^{\theta}\frac{1}{\sqrt{1-k^2\sin^2\phi}}\,d\phi$ is the incomplete elliptical integral of the first kind with parameter $m = k^2$. Identifying terms, it results that $m = k^2 = \frac{A}{A+c_1}$. Therefore, (8) is equivalent to

$$\pm\mathrm{F}\left(\theta\,|\,\frac{A}{A+c_1}\right) = (z+c_2)\sqrt{A+c_1} \quad (9)$$

Note that θ is the inverse function of $\mathrm{F}\left(\theta\,|\,k^2\right) = u$, that is, $\theta(z) = F^{-1}\left(u\,|\,k^2\right)$. So, the analytical solution of the differential equation (5) can be expressed making use of the Jacobi elliptic functions, in particular

$$\theta(z) = \pm\,\mathrm{am}\left((z+c_2)\sqrt{A+c_1}\,|\,\frac{A}{A+c_1}\right) \quad (10)$$

where $\mathrm{am}\left(u\,|\,k^2\right)$ is the Jacobi amplitude function, and c_1 and c_2 are constants of integration that meet the boundary conditions $\theta(z=0) = \theta_p = \pm\,\mathrm{am}\left(c_2\sqrt{A+c_1}\,|\,\frac{A}{A+c_1}\right)$ and $\theta(z=d) = \theta_p = \pm\,\mathrm{am}\left((\mathrm{d}+c_2)\sqrt{A+c_1}\,|\,\frac{A}{A+c_1}\right)$.

A. PIECEWISE ANALYTICAL FUNCTION

Let us suppose $c_1 = 0$ in an initial stage. From equation (8), it is clear that

$$z(\theta) = \pm\frac{1}{\sqrt{A}}\int_{\phi=\theta_p}^{\theta}\frac{1}{\cos\phi}\,d\phi - c_2 \tag{11}$$

After evaluating the integral, we obtain

$$z(\theta) = \pm\frac{1}{\sqrt{A}}\left[\ln\left(\tan\theta + \sec\theta\right) - \theta_p'\right] - c_2 \tag{12}$$

where $\theta_p' = \ln\left(\tan\theta_p + \sec\theta_p\right)$. For the case of the positive sign in (12), $+\text{am}\left(u \mid k^2\right)$ is a strictly increasing function in the range $z \in [0, d]$, and the negative sign, $-\text{am}\left(u \mid k^2\right)$, is its reflection on the y-axis. Due to the form of both functions, it seems that $+\text{am}\left(u \mid k^2\right)$ is the solution of the approximated differential equation (5) in the interval $z \in [0, \frac{d}{2}]$ and a z-axis shifted function $-\text{am}\left(u_{\text{shifted}} \mid k^2\right)$ in the interval $z \in [\frac{d}{2}, d]$. Note that the constant of integration c_2, which is directly related to z in (12), is responsible of moving the function $-\text{am}\left(u_{\text{shifted}} \mid k^2\right)$. Separating both solutions with their respective constants of integration, equation (12) stays as

$$\text{z}(\theta) = \begin{cases} \dfrac{\ln\left(\tan\theta + \sec\theta\right) - \theta_p'}{\sqrt{A}} - c_{2+} & \text{if} \quad 0 \le \text{z} \le \frac{d}{2} \\ -\dfrac{\ln\left(\tan\theta + \sec\theta\right) - \theta_p'}{\sqrt{A}} - c_{2-} & \text{if} \quad \frac{d}{2} \le \text{z} \le d \end{cases} \tag{13}$$

According to this, as the first of the boundary conditions ($\theta(z = 0) = \theta_p$, which is the inverse of $z(\theta = \theta_p) = 0$) is applied on $z = 0$, the constant of integration c_{2+} must be null. The second boundary condition $z(\theta = \theta_p) = d$, referred to $z(\theta)$, must be evaluated on the lower term of expression (13), which leads to $c_{2-} = -d$. Note that we are interested in obtaining $\theta(z)$, which is the inverse function of (13). In this particular case, $\theta(z)$ can be analytically isolated. After replacing c_{2+} and c_{2-} by their calculated values, the analytical equation that expresses the tilt angle of directors in a nematic LC is of the form

$$\theta(z) = \begin{cases} 2\tan^{-1}\left(e^{z\sqrt{A}+\theta_p'}\right) - \frac{\pi}{2} & \text{if } 0 \le z \le \frac{d}{2} \\ 2\tan^{-1}\left(e^{-(z-d)\sqrt{A}+\theta_p'}\right) - \frac{\pi}{2} & \text{if } \frac{d}{2} \le z \le d, \end{cases} \tag{14}$$

that fulfills the boundary conditions $\theta(z = 0) = \theta_p = \theta(z = d)$, is continuous in the interval $z \in [0, d]$, but not derivable at $z = \frac{d}{2}$. Therefore, it cannot be considered as a solution of (5). Anyway, as will be seen in later figures, it approximates in a good and easy manner the behavior of, not only the simplified differential equation (case $k_{11} \approx k_{33}$), but also the original differential equation (2).

B. ANALYTICAL FUNCTION

The previous expression is not derivable in the central value, $z = \frac{d}{2}$, since it is defined in these two pieces. However, this can be neglected as the bias voltage is increased. In the case of needing an accurate characterization at the center of the material, a new analytical definition can be obtained, at the expense of the accuracy of the value at the boundaries. This modification is basically built by adding the two pieces of the piecewise function and subtracting the maximum value of its image, $\theta_{max} = \frac{\pi}{2}$. That is,

$$\theta(z) = 2\tan^{-1}\left(e^{z\sqrt{A}+\theta_p'}\right) + 2\tan^{-1}\left(e^{-(z-d)\sqrt{A}+\theta_p'}\right) - \frac{3\pi}{2} \tag{15}$$

Despite offering good results and being derivable, note that (15) does not satisfy the boundary conditions. In order to satisfy them, we replace $\frac{3\pi}{2}$ by a term c in equation (15). If we impose $\theta(z = 0) = \theta(z = d) = \theta_p$ then, the term c must be equal to

$$c = \theta_p - 2\tan^{-1}\left(e^{\theta_p'}\right) - 2\tan^{-1}\left(e^{d\sqrt{A}+\theta_p'}\right) \tag{16}$$

which is approximately $c \approx -\frac{3\pi}{2}$. Consequently, equation (15) is modified to

$$\theta(z) = 2\tan^{-1}\left(e^{z\sqrt{A}+\theta_p'}\right) + 2\tan^{-1}\left(e^{-(z-d)\sqrt{A}+\theta_p'}\right) + c \tag{17}$$

The effect of c in equation (17) is to compensate, in any case, the term of the piecewise function that should not be acting in the wrong interval. That is, $2\tan^{-1}\left(e^{-(z-d)\sqrt{A}+\theta_p'}\right) - \frac{\pi}{2}$ in $z \in [0, \frac{d}{2}]$ and $2\tan^{-1}\left(e^{z\sqrt{A}+\theta_p'}\right) - \frac{\pi}{2}$ in $z \in [\frac{d}{2}, d]$. It also smooths the midpoint $\frac{d}{2}$ and makes the function derivable.

A comparison among the solutions of the initial differential equation, its approximation without the squared first derivative (both done with the 'bvp4c' solver implemented in Matlab), the calculated analytical piecewise function (14) and the derivable analytical function (17) is represented in Fig. 3. In most cases, the maximum error in the approach is lower than 2°on average, which means that the proposed solutions are acceptable for practical applications. Nevertheless, when the bias voltage V reaches lower levels, as shown in Fig. 3c, the error in the middle of the z interval ($z = \frac{d}{2}$) is much higher in the case of the piecewise function.

Fig. 4 shows a comparison between the error of the piecewise solution (14) and the derivable analytical function (17), when comparing them with the original differential equation (2) and its no squared derivative approximation (4). As observed in Fig. 4a and Fig. 4b, the error of both analytical expressions practically overlaps each others when the applied voltage is high enough. When the potential drop is under 5 V, the error goes up strongly near the midpoint $\frac{d}{2}$ with the piecewise function, reaching almost 20° when the polarization voltage is 3 V, which does not happen with the derivable analytical expression (17). The appendix shows an alternative manner to validate the analytical approach.

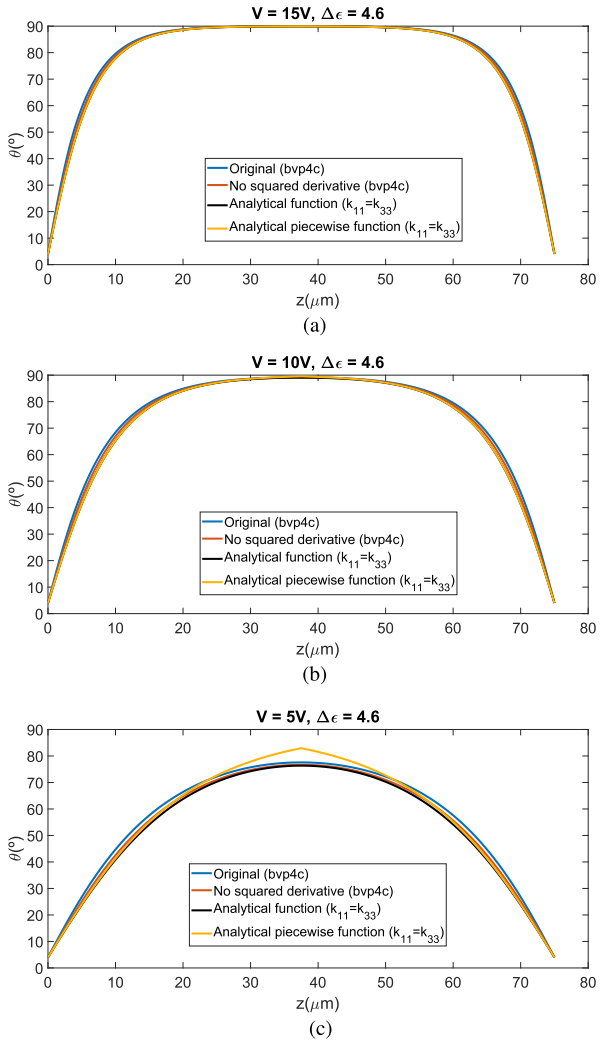

FIGURE 3. Comparison among the solutions of the original differential equation (2), its first approximation (both numerically solved with 'bvp4c' in MATLAB), the piecewise solution (14) (orange line) and the derivable analytical function (17) (black line), when V = 15 V (a), V = 10 V (b) and V = 5 V (c) ($\Delta\varepsilon = 4.6$, $k_{11} = 24$ pN, $k_{33} = 34.5$ pN and $\theta_p = 4°$). (a) A set of different solutions when V = 15 V. (b) A set of different solutions when V = 10 V. (c) A set of different solutions when V = 5 V.

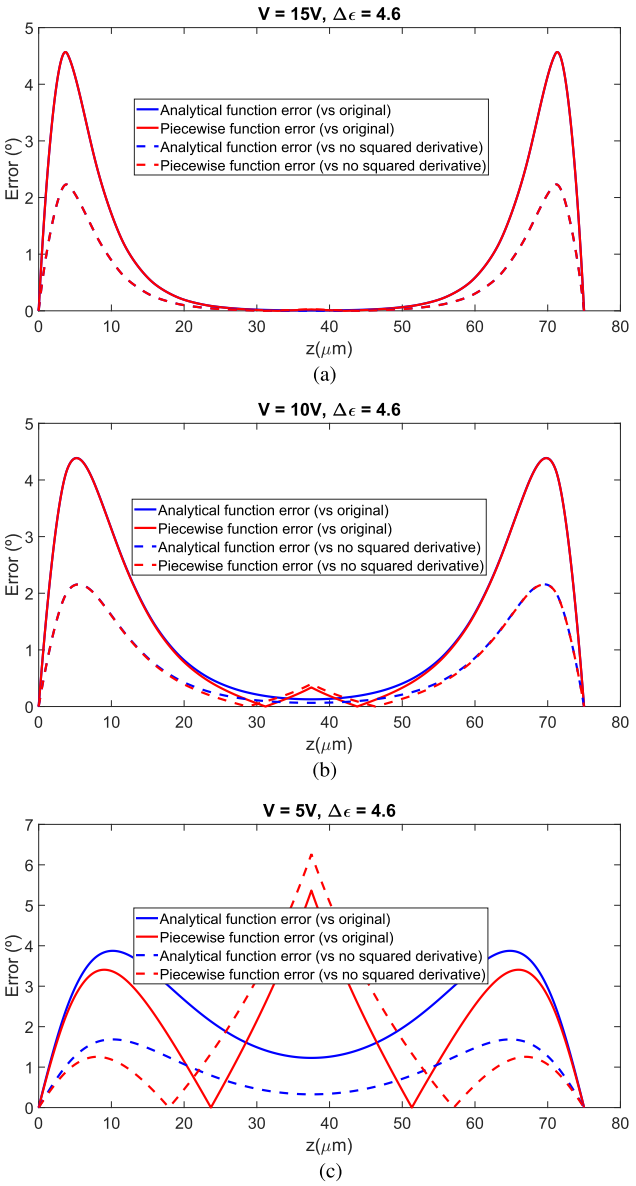

FIGURE 4. Comparison between the error of the piecewise solution and the derivable analytical function, when V = 15 V (a), V = 10 V (b) and V = 5 V (c) ($\Delta\varepsilon = 4.6$, $k_{11} = 24$ pN, $k_{33} = 34.5$ pN and $\theta_p = 4°$). (a) Error of both analytical solutions when V = 15 V. (b) Error of both analytical solutions when V = 10 V. (c) Error of both analytical solutions when V = 5 V.

Fig. 5 shows the piecewise and the derivable analytical expressions as a function of the bias voltage V. The displayed results are consistent with those provided in [20]. The error committed by the piecewise function when V is low is much greater than the one of the derivable function, which makes us choose the second option as the best approximation. On the other hand, when the bias voltage is high enough the error of both analytical expressions seems to converge to the same value. Apart from that, note also in general that the bigger V, the bigger is the director tilt angle.

Another parameter of interest, especially when working with the liquid crystal as a tunable dielectric, is the average director tilt angle θ_m. In essence, it can be calculated from (17) as

$$\theta_m = \frac{1}{d}\int_{z=0}^{d} \theta(z)\, dz \tag{18}$$

which leads to a difficult expression that is function of the elastic constants and the bias voltage.

In Fig. 6, this value is presented as a function of the bias voltage for the analytical and piecewise function. Note that when either the bias voltage V or dielectric anisotropy $\Delta\varepsilon$ increase, θ_m rises too. It can also be seen in the graph the average tilt angle saturates in both traces for high voltage values, especially when the dielectric anisotropy is high.

C. SELF-IMPLEMENTED SHOOTING METHOD

In general, nonhomogeneous boundary problems like (5) can have infinite solutions, one, or none (as in our case). The

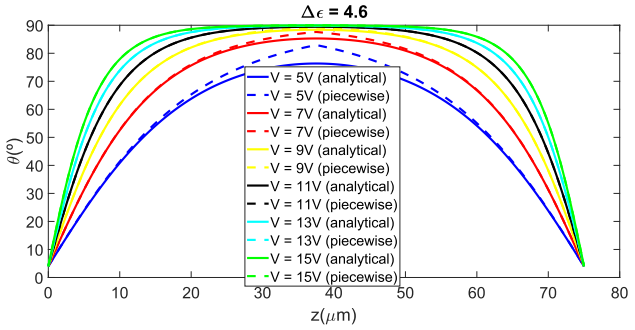

FIGURE 5. Analytical solutions for different bias voltages ($\Delta\varepsilon = 4.6$, $k_{33} = 34.5$ pN, $\theta_p = 4°$).

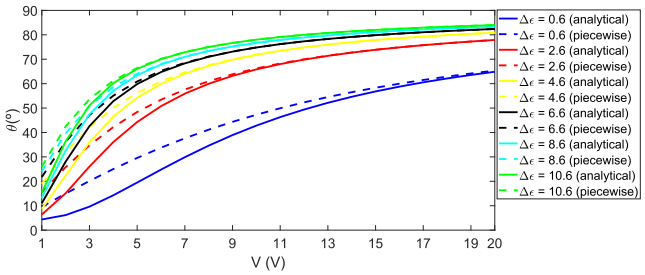

FIGURE 6. Average director tilt angle, as a function of bias voltage, for different dielectric anisotropy values ($k_{33} = 34.5$ pN, $\theta_p = 4°$).

shooting method try to solve these problems looking for a derivative condition such that boundary conditions are fulfilled. In this particular problem, maintaining fixed the first boundary condition $\theta(z = 0) = \theta_p$, we will try a first derivative condition, of the form $\theta'(z = 0) = s$, that meets the second boundary condition $\theta(z = d) = \theta_p$. In this context, it would be interesting to be able to estimate in what range does s move. As we already own information about the solution (Jacobi amplitude function), by derivating it and particularizing at $z = 0$, we will estimate $\theta'(0)$. The result of derivating (10) is

$$\theta'(z) = \pm\left(\sqrt{A + c_1}\right) \mathrm{dn}\left(z\sqrt{A + c_1} + \theta_p \mid \frac{A}{A + c_1}\right) \quad (19)$$

where $\mathrm{dn}(u \mid k^2)$ is the Jacobi delta amplitude function [27]. A property [29]–[31] of the delta amplitude function is that $\mathrm{dn}\left(0|k^2\right) = 1$. Since $\theta_p \approx 0$, the initial condition on the first derivate (19) is

$$\theta'(0) = \pm\left(\sqrt{A + c_1}\right) \mathrm{dn}\left(\theta_p \mid \frac{A}{A + c_1}\right) \approx +\left(\sqrt{A + c_1}\right) \quad (20)$$

where the minus sign has been neglected because we already known that $\theta(z)$ is a increasing function at $z = 0$, which implies a positive first derivative. According to this, it seems a good starting point to search values of s nearby $\sqrt{A}$. In Fig. 7, the value of the function $\theta(z)$ at $z = d$ has been plotted versus different values of the first derivative at $z = 0$, enclosed in the range $[0, 2\sqrt{A}]$. There are three solutions of the differential

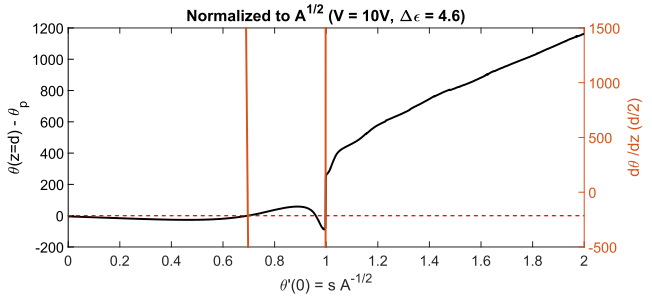

FIGURE 7. The functions $\theta(z = d) - \theta_p$ (black) and $\theta'(z = \frac{d}{2})$ (orange) for different values of $\theta'(0) = s$, normalized to $\sqrt{A}$ ($\Delta\varepsilon = 4.6$, $k_{33} = 34.5$ pN, $\theta_p = 4°$, V = 10 V).

TABLE 1. Normalized values ($\frac{s}{\sqrt{A}}$) of the equivalent problem with initial conditions $\theta(z = 0) = \theta_p$ and $\theta'(z = 0) = s$, for different bias voltages and dielectric anisotropies ($k_{33} = 34.5$ pN, $\theta_p = 4°$).

$\Delta\varepsilon$ \ V (V)	5	10	15
2.6	0.85230	0.995701	0.99770917
4.6	0.96450	0.997593	0.99778182
6.6	0.98691	0.99773575	0.9978010504

equation in the equivalent problem that satisfy the boundary condition $\theta(z = \theta_p)$. As expected, only one of them is of our interest. Note also that all solutions are placed nearby $\sqrt{A}$.

Here, it arises the question of how to systematically determine which is the solution we are looking for. This can be achieved by imposing another restriction on the function or in its derivatives. As the analytical and numerical results prove, the function $\theta(z)$ has a critical point (a maximum) at the midpoint $z = \frac{d}{2}$, that is, $\theta'(z = \frac{d}{2}) = 0$. Therefore, the initial conditions of the equivalent problem (solved by the shooting method) that returns us the same solutions are

$$\begin{cases} \theta(z = 0) = \theta_p \\ \theta'(z = 0) = s \\ \theta'(z = \frac{d}{2}) = 0 \\ \left(\theta''(z = \frac{d}{2}) < 0\right) \end{cases} \quad (21)$$

The sought solution will be the one whose $\theta'(z = 0) = s$ causes the boundary condition $\theta(z = 0) = \theta_p$ to be satisfied and at the same time meets $\theta'(z = \frac{d}{2}) = 0$. That is to say, we must graph together $\theta(z = d) - \theta_p$ and $\theta'(z = \frac{d}{2})$ vs different values of s and find when both coincide and cross zero. Naturally, we have to verify that the critical point is effectively a maximum, checking that $\theta''(z = \frac{d}{2}) < 0$.

As shown in Fig. 7, two of the three possible solutions that meet the boundary conditions (when V = 10 V) also have a critical point at $\frac{d}{2}$. These ones have been plotted in Fig. 8. In the first solution (blue line), the midpoint coincides with a local minimum, while in the second solution (red line), it coincides with the absolute maximum sought.

In Table 1, we tabulate some normalized values ($\frac{s}{\sqrt{A}}$) of the equivalent initial value problem (5) and (21) that guarantee the same results obtained before with analytical and

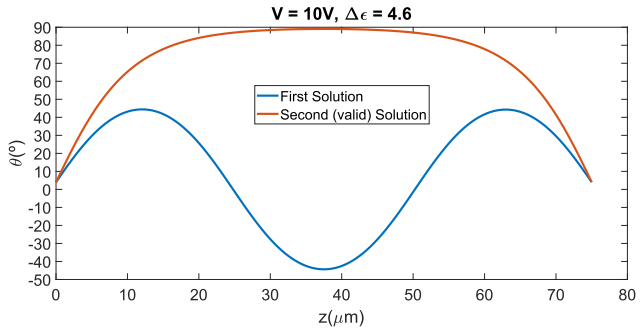

FIGURE 8. Both solutions of equation (5) with a critical point at the midpoint $\frac{d}{2}$ that fulfills the boundary conditions, after applying the self-implemented shooting method ($\Delta\varepsilon = 4.6$, $k_{33} = 34.5$ pN, $\theta_p = 4°$, V = 10 V).

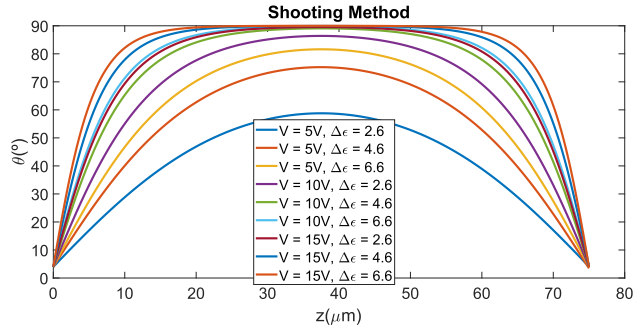

FIGURE 9. Numerical solution, with the self-implemented shooting method, of the tilt angle of directors in the liquid crystal for different values of the bias voltage and the dielectric anisotropy.

numerical approaches (check Fig. 3 and Fig. 5). These numbers were achieved by applying the commented above, and they are particularized to three different voltages and three values of the dielectric anisotropy in the liquid crystal. Note that the greater the bias voltage is, the greater the number of solutions which have a critical point in the midpoint $\frac{d}{2}$, and the greater is the number of decimal digits needed to specify the correct solution.

Fig. 9 represents the solutions referred to in Table 1. As previously commented, the bigger the voltage or the dielectric anisotropy in the LC, the bigger the director tilt angle is. Note also that the average director tilt angle increases quicker with the bias voltage than the dielectric anisotropy, because of the quadratic dependence of the electric field in (5) ($A = \frac{\varepsilon_0 \Delta\varepsilon E^2}{k_{33}}$) rather than the linear of the latter.

V. EXAMPLE OF THE USE OF THE ANALYTICAL EQUATION

Let us suppose that the electrical behavior of a given 200 μm liquid crystal ($\varepsilon_{//} = 3.3$, $\varepsilon_{\perp} = 2.5$, $\Delta\varepsilon = 0.8$, $k_{11} = 10$ pN, $k_{33} = 18$ pN, $\theta_p = 4°$) must be determined. As depicted in Section II, this is achieved by completing the permittivity tensor of expression (1). There is an electrical potential difference of 18 V between the metallic plates in which the LC is confined. Therefore, the module of the electric field results $E = \frac{V}{d} = 9 \cdot 10^4$ V/m. The average director tilt angle will

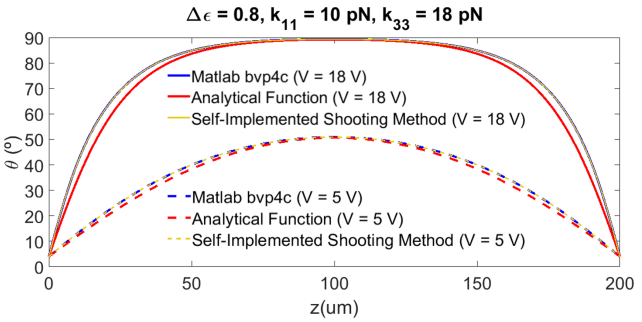

FIGURE 10. Comparison among the solutions of the differential equation according to the bvp4c solver implemented in Matlab, the analytical expression, and the self-implemented shooting method. Blue and yellow lines overlap each other.

be oriented almost perpendicular to the metallic plates due to elevated bias voltage applied in the structure.

From $\theta_p' = \ln\left(\tan\theta_p + \sec\theta_p\right)$, it is determined that $\theta_p' = 0.0699$. Another parameter that conforms the analytical expression (17) is A, which takes a value of $A = \frac{\varepsilon_0 \Delta\varepsilon E^2}{k_{33}} = 3.186 \cdot 10^9 \frac{\text{F·V}}{\text{N·m}^3}$. The remaining parameter, c, is extracted from equation (16), leading to $c = -4.7124$. Therefore, the analytical function for this particular case is

$$\theta(z) = -4.7124 + 2\tan^{-1}\left(e^{z\sqrt{3.186\cdot 10^9}+0.0699}\right) + 2\tan^{-1}\left(e^{-(z-200\cdot 10^{-6})\sqrt{3.186\cdot 10^9}+0.0699}\right)$$

On the other hand, the use of our self-implemented shooting method shows that the initial condition of the equivalent problem is $\frac{s}{\sqrt{A}} = 1.33568151$. The analytical function and the numerical solutions (Matlab and the self-implemented shooting method) are subsequently plotted in Fig. 10. In order to prove the robustness of the analytical expression, a comparison for $V = 5$ V has been also included in Fig. 10. Note that despite using different voltage values and that $k_{11} \approx k_{33}$ ($a = 0.56$), the concordance between the numerical solutions and the analytical expression is noticeable.

The average director tilt angle θ_m is calculated in the case where $V = 18$ V according to the mean value of the analytical expression. This leads to $\theta_m = 72.15°$. If the average director is calculated according to the numerical results, it takes a value of $\theta_m = 74.38°$. Therefore, the average error committed in the approximation is 2.23°(3 %). The average director tilt angle is finally used to form the permittivity tensor that fully characterizes the electrical behavior of the liquid crystal. Making use of equation (1) and the values referred in this section, the permittivity tensor is

$$\bar{\bar{\varepsilon}} = \begin{pmatrix} 2.50 & 0 & 0 \\ 0 & 2.58 & 0.23 \\ 0 & 0.23 & 3.22 \end{pmatrix}$$

The permittivity tensor is the parameter needed by any electromagnetic simulator to perform a more realistic model of the structure or to analyze other terms of interest, such as the phase shift provided by the LC.

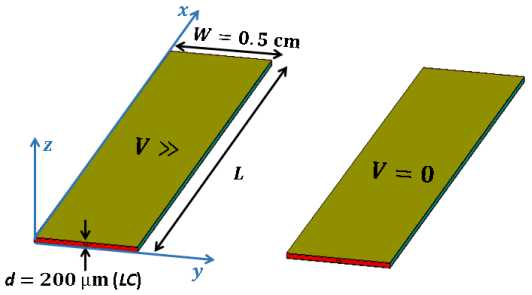

FIGURE 11. Simulation in *CST Microwave Studio* of the GT3-23001 liquid crystal [28] confined between metallic plates when polarized with the extreme voltages.

VI. ELECTROMAGNETIC SIMULATION

A parallel-plate waveguide filled with a lossy liquid crystal acting as tunable dielectric (the part marked in red of the device shown in Fig. 1) is tested in *CST Microwave Studio*. To this effect, a GT3-23001 liquid crystal mixture ($\varepsilon_{//} = 3.3$, $\varepsilon_{\perp} = 2.5$, $\tan\delta_{//} = 0.0038$, $\tan\delta_{\perp} = 0.0143$ @ 19 GHz) [28] of thickness 200 μm is modeled in the simulator through the permittivity tensor of equation (1). Note that the parallel permittivity indicates the orientation of the director $\hat{n}$ in the extreme cases, where the polarization voltage V can take either an elevated value or zero. The tensors from both cases only include elements in their main diagonal. The permittivity tensor when $V = 0$ is calculated as

$$\bar{\bar{\varepsilon}}_{V=0} = \begin{pmatrix} \varepsilon_{\perp} & 0 & 0 \\ 0 & \varepsilon_{//} & 0 \\ 0 & 0 & \varepsilon_{\perp} \end{pmatrix} \tag{22}$$

with the average director oriented in the y-axis (parallel to the plates). The permittivity tensor when $V >>$ is

$$\bar{\bar{\varepsilon}}_{V>>} = \begin{pmatrix} \varepsilon_{\perp} & 0 & 0 \\ 0 & \varepsilon_{\perp} & 0 \\ 0 & 0 & \varepsilon_{//} \end{pmatrix} \tag{23}$$

with the average director oriented in the z-axis (perpendicular to the plates). Figure 11 depicts the simulated structure and its dimensions. Losses due to the presence of the liquid crystal have been taken into account in the simulation by means of the loss tangent diagonal tensor.

The electric field is oriented along the z-axis in the LC. Since the parallel permittivity is higher than the perpendicular one, the structure must provide a higher phase shift if the average director is positioned in the same direction that the electric field. This is achieved by applying a high potential difference ($V >>$) between the metallic plates. On the other hand, the structure must provide a lower phase shift if the average director is not oriented in the same axis that the electric field. This is achieved by applying a low potential difference. This fact is noticed in Fig. 12, where the continuous black line has a steeper slope along the frequency than the dashed black line. This means that a high polarization voltage causes greater phase shift. The same applies to the 2 cm waveguide section.

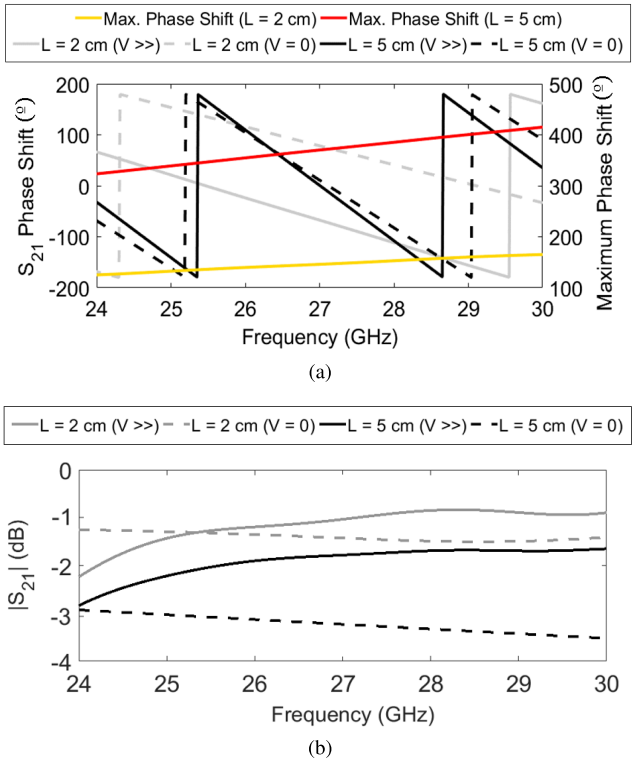

FIGURE 12. Transmission coefficient in the parallel-plate waveguide filled with GT3-23001 liquid crystal. (a) Maximum phase shift. (b) Transmission loss.

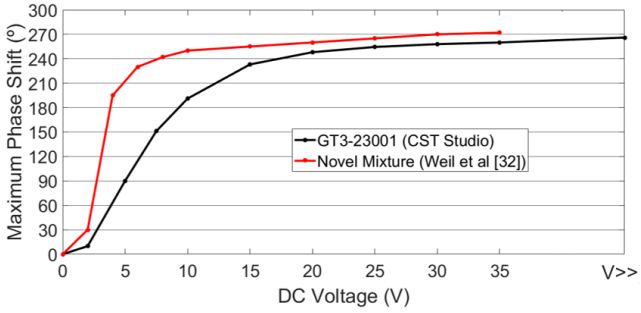

FIGURE 13. Comparison between the maximum phase shift observed at 20 GHz in the GT3-23001 LC mixture and the maximum phase shift measured in [32]. Both as a function of the bias voltage.

The magnitude and the phase of the transmission coefficient two parallel-plate waveguide sections of lengths 2 cm and 5 cm are plotted in Fig. 12. Red and yellow solid lines in Fig. 12a (they are referred to the right y-axis) mark the maximum phase shift range that can be achieved in the structure. The maximum phase shift already covers a entire turn (360°) at 26.3 GHz in the 5 cm waveguide. However, the transmission loss is up to 3 dB in this particular case. Note that the transmission loss is lower in the case of polarizing the liquid crystal with a higher bias voltage, since the parallel tangent loss is lower than the perpendicular one. On the other hand, a maximum phase shift of 140° can be obtained at 26.3 GHz in the 2 cm section with losses under 1.5 dB.

Fig. 13 presents the maximum phase shift at 20 GHz, associated to each bias voltage V, that the GT3-23001 LC mixture can provide. The analytical solution (17) has been used to obtain the permittivity tensor for each voltage value. Then, the permittivity tensor is introduced in the simulator and the phase shift is computed and compared with the results of [32]. Weil *et al.* [32] show that a maximum phase shift of 272° is experimentally achieved at 20 GHz in a 4.8 cm LC phase shifter. In our particular case, the maximum phase shift observed in CST Studio at 20 GHz is 266°, very close to 272°. Even though the maximum phase shift is similar in both cases, the red line has a steeper slope because of the use of a liquid crystal of slightly different characteristics in [32].

VII. CONCLUSION

This paper presents an analytical expression that models the tilt angle of liquid crystal (LC) directors in the nematic phase when a quasi-static electric field is applied. First of all, it is demonstrated that the original differential equation (2) could be simplified when working with high bias voltages into an easier expression, (4). A particular case of this equation arises when $k_{11} = k_{33}$ (a = 1), allowing us to reduce terms. It was proved that (5) has an analytical piecewise solution that is written by making use of the Jacobi amplitude function. From the piecewise function, it is found another analytical expression (17) that models with less error, lower than 2° on average, the tilt angle of directors in the liquid crystal. It is clearly seen as the analytical formula greatly simplifies the design process, as opposed to the tedious numerical methods depicted. Besides that, it is implemented a shooting method to obtain another numerical solution, different than the one provided by Matlab, in order to compare results. The correspondence between the three solutions is remarkable. Then, the average director tilt angle θ_m, necessary to form the full permittivity tensor $\bar{\bar{\varepsilon}}$ that characterizes completely the electrical properties of the liquid crystal, is obtained by integrating the calculated analytical functions. As expected, the bigger the bias voltage V or the dielectric anisotropy $\Delta\varepsilon$, the bigger θ_m is. Finally, an electromagnetic simulation in *CST MWS* is carried out to show the capabilities of the LC as a tunable device. It is depicted that only 5 cm of a commercial liquid crystal mixture are necessary to obtain a tunable phase shifter with losses below 3 dB at 26.3 GHz. 360°

APPENDIX. CHECKING THE VALIDITY OF THE ANALYTICAL APPROACH

A useful test to validate the results shown in the manuscript is to insert the analytical expression (17) into the original differential equation (eq. (2)). The result must be zero o very close to zero. Thus, we name by $f(z)$ to

$$f(z) = \left(k_{11}\cos^2\theta + k_{33}\sin^2\theta\right)\frac{d^2\theta}{dz^2} + (k_{33} - k_{11})\left(\frac{d\theta}{dz}\right)^2 \sin\theta\cos\theta + \beta\sin\theta\cos\theta$$

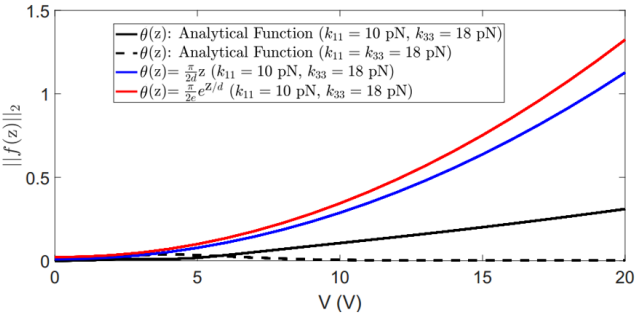

FIGURE 14. Norm of the function $f(z)$.

The norm of the function f, $||f(z)||_2$, gives us an image of how good the analytical solution is. The more closer to zero, the better the analytical approach is. Subsequently, we replace the analytical expression (17) into $f(z)$ and numerically calculate the value of the norm for different voltage and elastic constant values. Results are depicted in Fig. 14. The solid black line represents the norm of the analytical function for the case presented in Section V. The dashed black curve presents a similar approach, but with the elastic constants k_{11} and k_{33} being identical. The norm of both black curves is near to zero, which validates the analytical solution proposed in the manuscript. Concretely, note that the norm of the dashed black curve is practically zero. It is even lower than the solid black line, which makes sense as the analytical approach is defined in the manuscript for cases where $k_{11} \approx k_{33}$ ($k_{11} = k_{33} = 18$ pN). Besides, the norm is very high in those cases where $\theta(z)$ is not a solution of the differential equation (2). The blue and red curves represents the functions $\theta(z) = \frac{\pi}{2d}z$ and $\theta(z) = \frac{\pi}{2e}e^{z/d}$, respectively. Since z is enclosed between 0 and d, the range of both functions is in the interval $[0, \frac{\pi}{2}]$, as in the analytical approach. Both functions are put into scene to demonstrate that the norm quickly moves away from a null value if the considered function is not a valid solution.

REFERENCES

[1] M. Agiwal, A. Roy, and N. Saxena, "Next generation 5G wireless networks: A comprehensive survey," *IEEE Commun. Surveys Tuts.*, vol. 18, no. 3, pp. 1617–1655, 3rd Quart., 2016.

[2] M. Romagnoli *et al.*, "Graphene-based integrated photonics for next-generation datacom and telecom," *Nature Rev. Mater.*, vol. 3, pp. 392–414, Oct. 2018.

[3] Z. Gu *et al.*, "Resonant domain-wall-enhanced tunable microwave ferroelectrics," *Nature*, vol. 560, pp. 622–627, Aug. 2018.

[4] J. S. Gibson, X. Liu, S. V. Georgakopoulos, J. J. Wie, T. H. Ware, and T. J. White, "Reconfigurable antennas based on self-morphing liquid crystalline elastomers," *IEEE Access*, vol. 4, pp. 2340–2348, 2016.

[5] P. Yaghmaee, O. H. Karabey, B. Bates, C. Fumeaux, and R. Jakoby, "Electrically tuned microwave devices using liquid crystal technology," *Int. J. Antennas Propag.*, vol. 2013, Sep. 2013, Art. no. 824214.

[6] Y. Garbovskiy *et al.*, "Liquid crystal phase shifters at millimeter wave frequencies," *J. Appl. Phys.*, vol. 111, no. 5, p. 054504, Jan. 2012.

[7] G. Perez-Palomino *et al.*, "Design and experimental validation of liquid crystal-based reconfigurable reflectarray elements with improved bandwidth in F-band," *IEEE Trans. Antennas Propag.*, vol. 61, no. 4, pp. 1704–1713, Apr. 2013.

[8] O. H. Karabey, A. Gaebler, S. Strunck, and R. Jakoby, "A 2-D electronically steered phased-array antenna with 2×2 elements in LC display technology," *IEEE Trans. Microw. Theory Techn.*, vol. 60, no. 5, pp. 1297–1306, May 2012.

[9] W. Hu *et al.*, "Liquid crystal tunable mm wave frequency selective surface," *IEEE Microw. Wireless Compon. Lett.*, vol. 17, no. 9, pp. 667–669, Sep. 2007.
[10] A. Tamayo-Domínguez, J. M. Fernández-González, and M. Sierra-Pérez, "Groove gap waveguide in 3-D printed technology for low loss, weight, and cost distribution networks," *IEEE Trans. Microw. Theory Techn.*, vol. 65, no. 11, pp. 4138–4147, Nov. 2017.
[11] M. M. M. Ali, S. I. Shams, and A.-R. Sebak, "Printed ridge gap waveguide 3-dB coupler: Analysis and design procedure," *IEEE Access*, vol. 6, pp. 8501–8509, 2018.
[12] B. F. de Oliveira, P. P. Avelino, F. Moraes, and J. C. R. E. Oliveira, "Nematic liquid crystal dynamics under applied electric fields," *Phys. Rev. E, Stat. Phys. Plasmas Fluids Relat. Interdiscip. Top.*, vol. 82, no. 4, p. 041707, Oct. 2010.
[13] P. A. Cruz and M. F. Tomé, "Numerical simulation of director orientation of nematic liquid crystal in tumbling flows," in *Proc. V Eur. Conf. Comput. Fluid Dyn.*, Jun. 2010, pp. 1–19.
[14] J. B. Davies, S. Day, F. Di Pasquale, and F. A. Fernandez, "Finite-element modelling in 2-D of nematic liquid crystal structures," *Electron. Lett.*, vol. 32, no. 6, pp. 582–583, Mar. 1996.
[15] Z. Ge, T. X. Wu, R. Lu, X. Zhu, Q. Hong, and S.-T. Wu, "Comprehensive three-dimensional dynamic modeling of liquid crystal devices using finite element method," *J. Display Technol.*, vol. 1, no. 2, pp. 194–206, Dec. 2005.
[16] M. Yang, S. E. Day, and F. A. Fernández, "Modelling the optics of high resolution liquid crystal devices by the finite differences in the frequency domain method," in *Proc. Int. Workshop Electromagn., Appl. Student Innov. Competition*, May/Jun. 2017, pp. 141–143.
[17] F. A. Fernández *et al.*, "Accurate modelling of liquid crystal-based microwave devices," *Mol. Cryst. Liq. Cryst.*, vol. 619, p. 1, pp. 19–27, Oct. 2015.
[18] R.-H. Guan, Y.-B. Sun, and G.-S. Fu, "Response times in π-cell liquid crystal displays," *Liq. Cryst.*, vol. 35, no. 7, pp. 841–845, Aug. 2008.
[19] J. F. Algorri, V. Urruchi, and P. J. Pinzón, J. M. Sánchez-Pena, "Modeling electro-optical response of nematic liquid crystals by numerical methods," *ÓPTICA Pura Y Aplicada*, vol. 46,no. 4, pp. 327–336, Oct. 2013.
[20] G. Perez-Palomino *et al.*, "Accurate and efficient modeling to calculate the voltage dependence of liquid crystal-based reflectarray cells," *IEEE Trans. Antennas Propag.*, vol. 62, no. 5, pp. 2659–2668, May 2014.
[21] M. Liu, "Maxwell equations in nematic liquid crystals," *Phys. Rev. E, Stat. Phys. Plasmas Fluids Relat. Interdiscip. Top.*, vol. 50, no. 4, p. 2925, Oct. 1994.
[22] J. A. Reyes and R. F. Rodríguez, "Absorption effects in liquid crystal waveguides," *Phys. Rev. E, Stat. Phys. Plasmas Fluids Relat. Interdiscip. Top.*, vol. 68, p. 041707, Oct. 2003.
[23] B. J. Frisken and P. Palffy-Muhoray, "Freedericksz transitions in nematic liquid crystals: The effects of an in-plane electric field," *Phys. Rev. A, Gen. Phys.*, vol. 40, no. 10, pp. 6099–6102, Nov. 1989.
[24] R. H. Chen, *Liquid Crystal Displays: Fundamental Physics and Technology*. Hoboken, NJ, USA: Wiley, 2011.
[25] K. H. Fan-Chiang, S.-T. Wu, and S.-H. Chen, "Fringing-field effects on high-resolution liquid crystal microdisplays," *J. Display Technol.*, vol. 1, no. 2, pp. 304–313, Dec. 2005.
[26] X. Nie, H. Xianyu, R. Lu, T. X. Wu, and S.-T. Wu, "Pretilt angle effects on liquid crystal response time," *J. Display Technol.*, vol. 3, no. 3, pp. 280–283, Sep. 2007.
[27] A. D. Polyanin and A. V. Manzhirov, *Handbook of Integral Equations*, 2nd ed. Boca Raton, FL, USA: CRC Press, 2008.
[28] P. Yaghmaee, W. Withayachumnankul, A. K. Horestani, A. Ebrahimi, B. Bates, and C. Fumeaux, "Tunable electric-LC resonators using liquid crystal," in *Proc. IEEE Antennas Propag. Soc. Int. Symp. (APSURSI)*, Jul. 2013, pp. 382–383.
[29] J. V. Armitage and W. F. Eberlein, *Elliptic Functions*. Cambridge, U.K.: Cambridge Univ. Press, 2009.
[30] Y. L. Luke, "Approximations for elliptic integrals," *Math. Comput.*, vol. 22, no. 103, pp. 627–634, Jul. 1968.
[31] S. Liu, Z. Fu, S. Liu, and Q. Zhao, "Jacobi elliptic function expansion method and periodic wave solutions of nonlinear wave equations," *Phys. Lett. A*, vol. 289, nos. 1–2, p. 69–74, Oct. 2001.
[32] C. Weil *et al.*, "Ferroelectric- and liquid crystal-tunable microwave phase shifters," in *Proc. 33rd Eur. Microw. Conf.*, vol. 3, Oct. 2003, pp. 1431–1434.

ANTONIO ALEX-AMOR received the B.Sc. degree in telecommunication engineering from Universidad de Granada, in 2016, and the M.Sc. degree in telecommunication engineering from Universidad Politécnica de Madrid (UPM), in 2018, where he is currently pursuing the Ph.D. degree.

Since 2016, he has been with the Radiation Group, Signal, Systems and Radiocommunications Department, UPM. In 2018, he joined the Department of Language and Computer Science, Universidad de Málaga. His current research interests include the use of liquid crystal as tunable dielectric, radiofrequency energy harvesting systems, and higher symmetry structures.

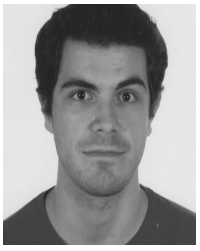

ADRIÁN TAMAYO-DOMÍNGUEZ was born in Madrid, Spain. He received the M.Sc. degree in telecommunication engineering from the Universidad Politécnica de Madrid, Madrid, in 2016, where he is currently pursuing the Ph.D. degree. His current research interests include RF circuits, liquid crystal as tunable dielectric, and gap waveguides applied on planar antenna applications oriented to 5G developing.

ÁNGEL PALOMARES-CABALLERO was born in Jaén, Spain, in 1994. He received the B.Sc. and M.Sc. degrees in telecommunication engineering from the Universidad de Granada, Spain, in 2016 and 2018, respectively, where he is currently pursuing the Ph.D. degree and has been with the Department of Signal Theory, Telematics and Communications, since 2017. His research interests include millimeter wave-antennas, gap waveguide, and optimization algorithms and structures with higher symmetries.

JOSÉ M. FERNÁNDEZ-GONZÁLEZ was born in Lausanne, Switzerland. He received the Diplôme d'Ingénieur en Électricité degree from the École Polytechnique Fédérale de Lausanne, Lausanne, in 2003, and the Ph.D. degree from the Universidad Politécnica de Madrid, Madrid, Spain, in 2009. In 2006, he joined the Centre de Recherches Poly-Grames, L'École Polytechnique de Montréal, Montreal, QC, Canada. In 2007, he joined the Chalmers University of Technology, Göteborg, Sweden, as a Guest Ph.D. Student. Since 2013, he has been an Assistant Professor with the Universidad Politécnica de Madrid. He has participated in more than 35 research projects and contracts. He has authored more than 90 publications in scientific journals, symposium proceedings, and seminars. He holds four patents. His current research interests include phased array antennas, RF circuits, and metamaterial structures with an emphasis on planar antenna applications.

PABLO PADILLA was born in Jaén, Spain, in 1982. He received the Telecommunication Engineer degree from the Technical University of Madrid (UPM), Spain, in 2005, and the Ph.D. degree from the Radiation Group, Signal, Systems and Radiocommunications Department, UPM, in 2009. In 2007, he was with the Laboratory of Electromagnetics and Acoustics, Ecole Polytechnique Fédérale de Lausanne, Switzerland, as an invited Ph.D. Student. In 2009, he carried out a postdoctoral stay at the Helsinki University of Technology. In 2009, he became an Assistant Professor with the Signal Theory, Telematics and Communications Department, Universidad de Granada. Since 2012, he has been an Associate Professor. He has authored more than 50 high-impact journal contributions and more than 40 contributions to international symposia. His research interests include a variety of areas of knowledge, related mainly to communication topics (radiofrequency devices, antennas, and propagation), network topics (wireless communication networks), and data exploration topics.

JUAN VALENZUELA-VALDÉS was born in Marbella, Spain. He received the degree in telecommunications engineering from the Universidad de Malaga, Spain, in 2003, and the Ph.D. degree from the Universidad Politécnica de Cartagena, Spain, in 2008. In 2004, he joined the Department of Information Technologies and Communications, Universidad Politécnica de Cartagena. In 2007, he joined EMITE Ing. as the Head of Research. In 2011, he joined the Universidad de Extremadura. In 2015, he joined Universidad de Granada, where he is currently an Associate Professor. He was a Co-Founder of Emite Ing., a spin-off company. His publication record is composed of more than 80 publications, including 40 JCR indexed articles, more than 30 contributions in international conferences, and seven book chapters. He also holds several national and international patents. His current research interests include wireless communications and efficiency in wireless sensor networks. He has also been awarded several prizes, including a national prize to the Best Ph.D. in mobile communications by Vodafone and the i-Patentes Award by the Spanish Autonomous Region of Murcia for innovation and technology transfer excellence.

ANTONIO PALOMARES received the Ph.D. degree in mathematics from the Universidad de Granada, Granada, Spain, in 2003, where he is currently an Associate Professor with the Department of Applied Mathematics.